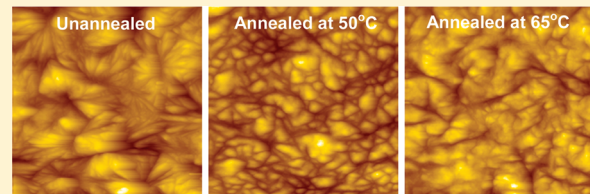


Unusual Cold Crystallization Behavior in Physically Aged Poly(L-lactide)

Bing Na,* Shufen Zou, Ruihua Lv, Mingbiao Luo, Huayan Pan, and Qiang Yin

Fundamental Science on Radioactive Geology and Exploration Technology Laboratory, School of Biology, Chemistry and Material Science, East China Institute of Technology, Fuzhou, 344000, People's Republic of China

ABSTRACT: A comparative study of cold crystallization behavior in poly(L-lactide) (PLLA) annealed below and just above the glass transition temperature (T_g) has been conducted. Annealing benefits the generation of local order and the subsequent cold crystallization process, which becomes significant in PLLA annealed just above T_g . Surprisingly, morphological observation reveals high density nuclei in PLLA annealed below T_g contrary to its relatively slow crystallization kinetics. This unusual crystallization behavior in physically aged PLLA arises from the retarded crystal growth rate because of incomplete recovery of reduced segmental mobility above T_g . In contrast, annealing just above T_g has little influence on the crystal growth rate, and the increased nucleation density alone accounts for the accelerated crystallization rate.



1. INTRODUCTION

Poly(L-lactide), PLLA, is a biodegradable aliphatic polyester with a low crystallization rate,^{1,2} and it is easy to obtain the amorphous state by quenching from the melt to temperatures below the glass transition temperature (T_g). Due to its thermodynamically unstable nature, the packing density and conformational structure of glassy PLLA tend to readjust toward equilibrium, giving rise to decreases in volume, enthalpy, and segmental mobility. This process is termed as physical aging and has a remarkable influence on properties of glassy PLLA such as density, yield strength, and modulus.^{3–6} Besides, it has been reported that, similar to what has been observed in amorphous poly(ethylene terephthalate), PET,^{7–9} the cold crystallization rate of glassy PLLA at temperatures above T_g can be enhanced with physical aging, apart from the shortening of the crystallization induction period.^{10,11} It arises from a significant increase in the nucleation rate and number of nuclei, correlating with the generation of energy-favorable conformers and in particular ordered domains in the physically aged PLLA. The ordered domains formed during physical aging can persist above T_g to some extent, as a result of incomplete recovery of enthalpy, and thus act as athermal nuclei to trigger cold crystallization in a relatively short period.

So far, only nucleation density is taken into account for the accelerated cold crystallization kinetics in physically aged PLLA,^{10,11} and the other factor, i.e., crystal growth rate, is seldom concerned. Because of high viscosity, crystal growth at temperatures not far above T_g is dominated by chain diffusion that is related to the segmental mobility. To our knowledge, physical aging can reduce the segmental mobility in glassy PLLA,^{3–6} manifested by the increase in modulus/strength and glass transition temperature. Thus, a question arises: can the reduced segmental mobility in the physically aged PLLA be recovered entirely while it is being heated above T_g where cold

crystallization takes place? In other words, it remains unclear whether physical aging has an influence on the segmental mobility and crystal growth rate during cold crystallization. A possible answer is given by cold crystallization of physically aged PET, in which the crystallization rate is retarded due to reduced segmental mobility on physical aging.⁸ The crystallization rate is contributed to by both nucleation density and crystal growth rate; nevertheless, individual information regarding nucleation and growth with respect to reduced segmental mobility is out of hand in the case of physically aged PET.

To clarify this, a comparative study of cold crystallization behavior in amorphous PLLA annealed below and just above T_g was conducted. Compared with virgin PLLA, accelerated cold crystallization is indeed observed in both annealed PLLA samples, irrespective of annealing temperature, originating from the increased nucleation density. However, the crystallization rate is incompatible with nucleation density with respect to annealing temperature. This enables us to deduce that the crystal growth rate is retarded in the physically aged PLLA, as a result of incomplete recovery of reduced segmental mobility above T_g .

2. EXPERIMENTAL SECTION

2.1. Materials and Sample Preparation. The PLLA, supplied by Natureworks, had a melt flow index of about 75 g/10 min and a relative viscosity of 2.5, respectively. Films for the following characterizations were cast from PLLA solution in chloroform, followed by drying in a vacuum oven at 40 °C for 48 h to remove residual solvent. To erase previous thermal history, as-cast films

Received: June 28, 2011

Revised: August 7, 2011

Published: August 18, 2011

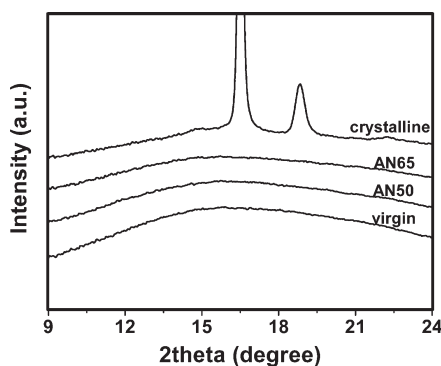


Figure 1. XRD profiles of virgin and annealed PLLA. For comparison the profile of fully crystalline sample is also included.

were first melted on a hot stage at 190 °C for 5 min and then quenched to room temperature. Through this procedure totally amorphous films with T_g values of about 60 °C were obtained and designated as virgin samples. Annealing of virgin samples below and just above T_g for 8 h was conducted at 50 and 65 °C, respectively. For convenience, samples annealed at 50 °C, for instance, were referred to AN50.

2.2. Differential Scanning Calorimetry (DSC). Cold crystallization behaviors were registered by a Perkin-Elmer DSC Pyris-1 in a nitrogen atmosphere. For nonisothermal experiments samples were heated from 30 to 190 °C at a rate of 10 °C/min. To study isothermal cold crystallization behavior, samples were rapidly heated to 85 °C and were held isothermally to achieve complete crystallization.

2.3. Atomic Force Microscopy (AFM). Crystal morphology was observed at ambient conditions by an atomic force microscope (AFM; SPI4000 Probe Station, SINT Instruments Co., Japan). The multimode AFM instrument was operated in a tapping mode, and height images were recorded. Prior to tests, virgin and annealed samples were held on a hot stage at 85 °C to achieve complete cold crystallization.

2.4. Fourier Transform Infrared Spectroscopy (FTIR). FTIR measurements were conducted by a Thermo Nicolet FTIR spectrometer at room temperature. Allowing for absorption coefficient differences with respect to various IR bands, transmission mode as well as attenuated total reflection (ATR) was adopted, respectively. IR spectra were collected with a resolution of 2 cm⁻¹ and a total of 32 scans were added.

2.5. X-ray Diffraction (XRD). XRD measurements were performed at room temperature on the diffraction workstation in the National Synchrotron Radiation Laboratory, Hefei, China. The wavelength of the X-rays was 0.154 nm, and the transmission mode was used.

3. RESULTS AND DISCUSSION

Figure 1 shows the XRD profiles of virgin and annealed PLLA, where the profile obtained from fully crystalline sample is also included for comparison. As expected, no crystals with long-range order are generated during the annealing process even at 65 °C. Herein, only diffusive diffraction associated with amorphous structure is observed in the virgin and annealed samples. Even so, local order may be created in the annealed PLLA, which is beyond the resolution of XRD measurements.

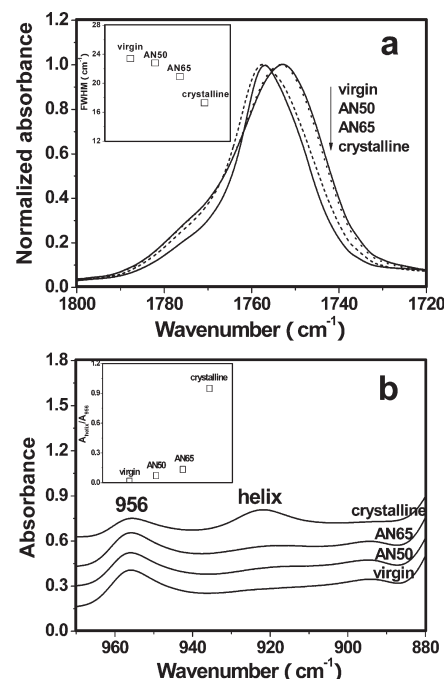


Figure 2. IR spectra in the (a) 1800–1720 and (b) 970–880 cm⁻¹ regions obtained with ATR and transmission mode, respectively, for virgin and annealed PLLA. For comparison the spectra of fully crystalline sample are also included. The insets in (a) and (b) represent the deduced full width at half-maximum (fwhm) and absorbance ratio A_{helix}/A_{956} , respectively.

In contrast, the FTIR technique, sensitive to local molecular environment,¹² is powerful enough to disclose the local order in PLLA. As depicted in Figure 2, structural changes on annealing are clearly demonstrated by the variation of IR bands in two indicated wavenumber regions. The band in the 1800–1720 cm⁻¹ region, related to the molecular packing, shifts to a higher wavenumber with respect to annealing especially in the AN65 samples.¹³ At the same time, the distribution of band intensity becomes narrow upon annealing, as quantitatively indicated by the full width at half-maximum (fwhm) in Figure 2a, inset. Similar results are presented when the band is inspected in the 940–900 cm⁻¹ region that is assigned to helix conformation.^{12,14} This helical band becomes obvious with annealing, and the quantitative analysis regarding the absorbance ratio of A_{helix}/A_{956} is given in Figure 2b, inset. Of note, the usage of A_{helix}/A_{956} , rather than A_{helix} is due to possible thickness differences in various samples, and the band at 956 cm⁻¹ is ascribed to the fully amorphous part in PLLA.^{12,13} Allowing that in both wavenumber regions the structural changes in the annealed samples follow the same tendency as the crystallization process, it is strongly suggested that annealing benefits the generation of local order or nuclei in PLLA through improving molecular packing and conformational ordering. Obviously, this event is highly favored in the AN65 samples where enough segmental mobility is gained above T_g . Rather, limited segmental motion in the physically aged PLLA can only produce local order to some extent in the AN50 ones.

Figure 3 shows the heating traces of virgin and annealed PLLA from the glassy state, where a distinct glass transition and cold crystallization behaviors are observed. During the glass transition

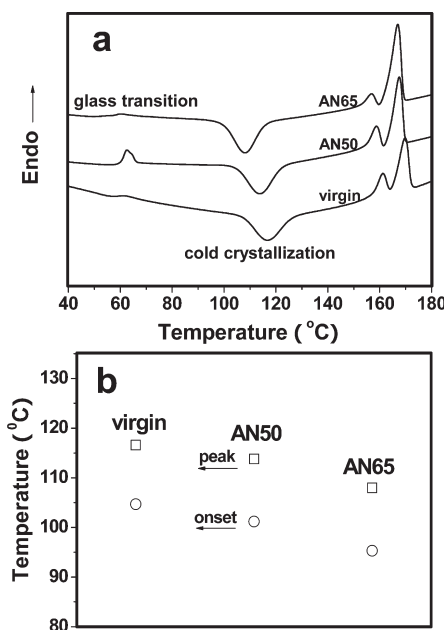


Figure 3. (a) DSC heating traces and (b) deduced onset and peak temperatures of cold crystallization for virgin and annealed PLLA.

region only the AN50 sample exhibits an endotherm, whereas a steplike change is presented in the virgin and AN65 samples. Moreover, a higher T_g is observed for the AN50 sample than for the virgin and AN65 counterparts. The appearance of the endotherm, rather than a steplike change, is a common observation in the physically aged polymers, and its molecular origin was an ongoing debate in the past. It had been ascribed to the significant recovery of free volume while aged polymers approach the glass transition region.¹⁵ However, a growing number of studies correlated it with the melting of local order formed during physical aging.^{3,16–18} Considering the FTIR results shown in Figure 2, we believe that the melting of local order in physically aged PLLA should be responsible for this endotherm. On the other hand, it seems that the local order generated during physical aging is quite different from that formed during annealing just above T_g . Local order prevails in the AN65 samples, as shown in Figure 2, but no endotherm associated with its melting is observed in the glass transition region. One possible reason is that local order in the AN65 samples has a higher thermal stability than that in AN50 ones and can withdraw the thermal destruction while approaching T_g . In other words, enough segmental mobility upon annealing above T_g could generate densely ordered domains in the AN65 samples. In contrast, local order with loose molecular organization is created in the AN50 samples because of limited segmental mobility during physical aging.

Certainly, ordered domains persisting above T_g is beneficial for the nucleation process due to a reduced energy barrier, as demonstrated by the low onset cold crystallization temperature in the AN65 samples. Meanwhile, the nucleation process also becomes easier for the AN50 samples than for the virgin ones, suggesting that local order formed during physical aging is not destroyed completely.^{10,11} That is, some fragments survive from the melting of initial local order, i.e., memory effect, similar to what has been claimed in the polymer crystallization from the melt without entirely erasing previous thermal history.^{19–21} Besides, the cold crystallization rate, qualitatively deduced from

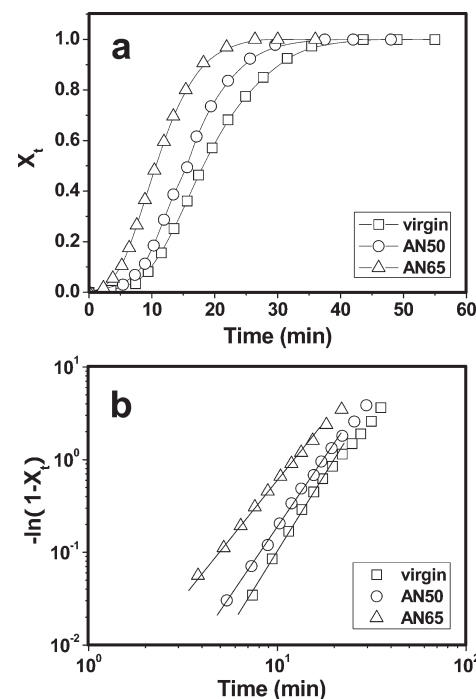


Figure 4. (a) Time-dependent relative crystallinity and (b) corresponding Avrami fitting obtained from virgin and annealed PLLA during cold crystallization at 85 °C.

Table 1. Deduced Cold Crystallization Parameters for Virgin and Annealed PLLA

samples	n	k (min ⁻ⁿ)	k ^{1/n} (min ⁻¹)	G (μm/min)
virgin	3.22	0.000 054 1	0.0473	0.147
AN50	2.98	0.000 194	0.0568	0.0534
AN65	2.54	0.001 72	0.0816	0.155

the peak temperature, follows the same tendency as the nucleation process with respect to annealing treatment.

To further demonstrate the cold crystallization kinetics with annealing, isothermal experiments were carried out, as shown in Figure 4. Consistent with the above nonisothermal results, a fast cold crystallization rate is presented in the annealed samples. The cold crystallization kinetics parameters, listed in Table 1, were deduced by the well-known Avrami equation as follows:

$$\log[-\ln(1 - X_t)] = \log k + n \log t \quad (1)$$

where X_t is the relative crystallinity at a given crystallization time t , n is the Avrami index, and k is the rate constant.

The Avrami index n , representing the crystal growth dimension, is around 3 for all samples. As demonstrated in another study,²² cold crystallization of PLLA usually follows a heterogeneous nucleation process, and thus the crystal growth dimension should be ~ 3 for all samples. This means that the growth mechanism is hardly altered by annealing. On the other hand, the deduced rate constant k is significantly increased with annealing. In order to compare the overall crystallization rate in the samples with different Avrami index n values, $k^{1/n}$ rather than k is adopted with consideration of unit consistency.²³ It is indicated that the overall crystallization rate is indeed enhanced especially in the AN65 samples. This accelerated crystallization is usually ascribed

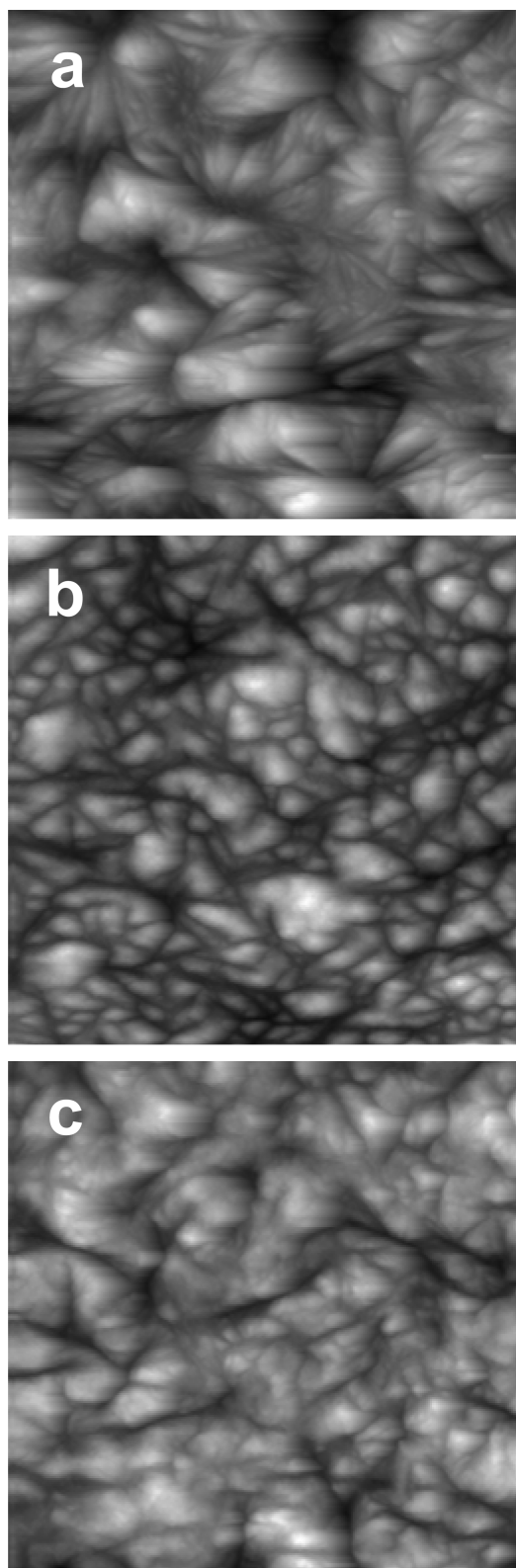


Figure 5. AFM images revealing crystal morphology of virgin (a) and annealed (b, AN50; c, AN65) PLLA after complete cold crystallization at 85 °C. The image size is $20 \times 20 \mu\text{m}^2$.

to the increased nucleation density. Since the overall crystallization rate, deduced from isothermal DSC measurements, is contributed by both nucleation density and crystal growth rate, it

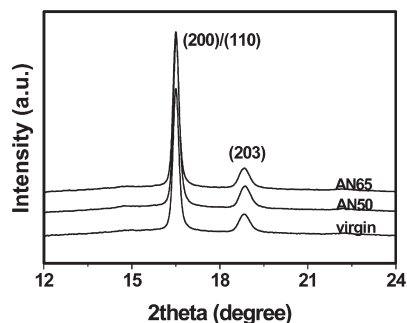


Figure 6. XRD profiles of virgin and annealed PLLA after complete cold crystallization at 85 °C.

is necessary to clarify their individual roles in the accelerated cold crystallization process of annealed PLLA.

To enable this, crystal morphology after complete cold crystallization was observed by AFM measurements, as shown in Figure 5. Surprisingly, higher nucleation density is presented in the AN50 samples than in the AN65 ones, contrary to the aforementioned change of overall crystallization rate with annealing temperature. This strongly suggests that nucleation density alone is not sufficient to account for the cold crystallization behavior in the AN50 samples. The other factor, i.e., crystal growth rate, might play a vital role during cold crystallization. Following the methods in other studies,^{22,24} the crystal growth rate G was estimated through eq 2:

$$G = R_m k^{1/n} \quad (2)$$

where R_m is the maximum radius of the spherulite after complete crystallization.

From the resulting values given in Table 1, it is indicated that annealing just above T_g has little effect on the crystal growth rate, whereas retarded crystal growth, by a factor of about 3, is exhibited in the physically aged samples. Two possible reasons could account for this. First, retarded crystal growth may arise from the different crystal modifications formed during cold crystallization.^{25,26} However, this possibility can be excluded when the XRD profiles of fully crystalline samples shown in Figure 6 are inspected. Herein, only characteristic reflections from the α' crystals of PLLA are observed,^{25,26} irrespective of annealing and annealing temperature. The other possibility could be the incomplete recovery of reduced segmental mobility in the physically aged PLLA above T_g where cold crystallization takes place. That is, chain diffusion at the growth front of crystals becomes slow due to reduced segmental mobility, which is responsible for the retarded crystal growth rate. It makes sense with further consideration that crystal growth at temperatures not far above T_g is dominated by chain diffusion because of high viscosity. Even so, fast nucleation and high density nuclei can be induced at the initial stage of cold crystallization in that some fragments with certain molecular ordering survive from the melting of initial local order. It, in turn, contributes to the slight increase in the overall cold crystallization rate in the AN50 samples. On the contrary, annealing just above T_g has little influence on the segmental mobility, as demonstrated by the glass transition shown in Figure 3, and thus the crystal growth rate in the AN65 samples is nearly identical to that of the virgin counterparts. The fast cold crystallization kinetics in the AN65 samples is solely resulted from the increase in the number of nuclei.

4. CONCLUSION

The unusual cold crystallization behavior in physically aged PLLA is well demonstrated by the combined analysis of crystallization kinetics and crystal morphology. Physical aging promotes the generation of high density nuclei, as a result of the memory effect of initial local order, but it suppresses crystal growth rate due to incomplete recovery of reduced segmental mobility above T_g . Even so, the overall cold crystallization rate, contributed by both nucleation density and growth rate, is enhanced to some extent in physically aged PLLA. This unique finding extends our insights into the relation between physical aging and the subsequent cold crystallization process in PLLA.

■ AUTHOR INFORMATION

Corresponding Author

*Fax: +86 794 8258320. E-mail: bingnash@163.com or bna@ecit.edu.cn.

■ ACKNOWLEDGMENT

This work is financially supported by the National Natural Science Foundation of China (Nos. 50973017 and 21004010) and the Project of Jiangxi Provincial Department of Education (Nos. GJJ08295 and GJJ11138).

■ REFERENCES

- (1) Sánchez, M. S.; Mathot, V. B. F.; Poel, G. V.; Ribelles, J. L. G. *Macromolecules* **2007**, *40*, 7989–7997.
- (2) Badrinarayanan, P.; Dowdy, K. B.; Kessler, M. R. *Polymer* **2010**, *51*, 4611–4618.
- (3) Liao, K.; Quan, D.; Lu, Z. *Eur. Polym. J.* **2002**, *38*, 157–162.
- (4) Kwon, M.; Lee, S. C.; Jeong, Y. G. *Macromol. Res.* **2010**, *18*, 346–351.
- (5) Aou, K.; Hsu, S. L.; Kleiner, L. W.; Tang, F. W. *J. Phys. Chem. B* **2007**, *111*, 12322–12327.
- (6) Pan, P.; Zhu, B.; Inoue, Y. *Macromolecules* **2007**, *40*, 9664–9671.
- (7) Lu, X.; Hay, J. N. *Polymer* **2000**, *41*, 7427–7436.
- (8) McGonigle, E. A.; Daly, J. H.; Gallagher, S.; Jenkins, S. D.; Liggett, J. J.; Olsson, I.; Pethrick, R. A. *Polymer* **1999**, *40*, 4977–4982.
- (9) Bove, L.; D'Aniello, C.; Gorras, G.; Guadagno, L.; Vittoria, V. *Polym. Bull.* **1997**, *38*, 579–585.
- (10) Pan, P.; Liang, Z.; Zhu, B.; Dong, T.; Inoue, Y. *Macromolecules* **2008**, *41*, 8011–8019.
- (11) Sánchez, F. H.; Mateo, J. M.; Colomer, F. J. R.; Sánchez, M. S.; Ribelles, J. L. G.; Mano, J. F. *Biomacromolecules* **2005**, *6*, 3283–3290.
- (12) Zhang, J.; Tsuji, H.; Noda, I.; Ozaki, Y. *J. Phys. Chem. B* **2004**, *108*, 11514–11520.
- (13) Meaurio, E.; López-Rodríguez, N.; Sarasua, J. R. *Macromolecules* **2006**, *39*, 9291–9301.
- (14) Na, B.; Tian, N.; Lv, R.; Li, Z.; Xu, W.; Fu, Q. *Polymer* **2010**, *51*, 563–567.
- (15) Pyda, M.; Wunderlich, B. *Macromolecules* **2005**, *38*, 10472–10479.
- (16) Pan, P.; Zhu, B.; Dong, T.; Yazawa, K.; Shimizu, T.; Tansho, M.; Inoue, Y. *J. Chem. Phys.* **2008**, *129*, 184902.
- (17) Na, B.; Lv, R.; Zou, S.; Li, Z.; Tian, N.; Fu, Q. *Macromolecules* **2010**, *43*, 1702–1705.
- (18) Qian, R.; Shen, D.; Sun, F.; Wu, L. *Macromol. Chem. Phys.* **1996**, *197*, 1485–1493.
- (19) Stribeck, N.; Nöchel, U.; Almendárez Camarillo, A.; Roth, S. V.; Dommach, M.; Bösecke, P. *Macromolecules* **2007**, *40*, 4535–4545.
- (20) Xu, J.; Ma, Y.; Hu, W.; Rehahn, M.; Reiter, G. *Nat. Mater.* **2009**, *8*, 348–353.
- (21) Na, B.; Wang, Y.; Zhang, Q.; Fu, Q. *Polymer* **2004**, *45*, 6245–6260.
- (22) Sakai, F.; Nishikawa, K.; Inoue, Y.; Yazawa, K. *Macromolecules* **2009**, *42*, 8335–8342.
- (23) Grady, B. P.; Pompeo, F.; Shambaugh, R. L.; Resasco, D. E. *J. Phys. Chem. B* **2002**, *106*, 5852–5858.
- (24) Nam, J. Y.; Ray, S. S.; Okamoto, M. *Macromolecules* **2003**, *36*, 7126–7131.
- (25) Zhang, J.; Duan, Y.; Sato, H.; Tsuji, H.; Noda, I.; Yan, S.; Ozaki, Y. *Macromolecules* **2005**, *38*, 8012–8021.
- (26) Kawai, T.; Rahman, N.; Matsuba, G.; Nishida, K.; Kanaya, T.; Nakano, M.; Okamoto, H.; Kawada, J.; Usuki, A.; Honma, N.; Nakajima, K.; Matsuda, M. *Macromolecules* **2007**, *40*, 9463–9469.